



ELSEVIER

Available online at www.sciencedirect.com



Physics Procedia 3 (2010) 373–380

**Physics
Procedia**

www.elsevier.com/locate/procedia

International Congress on Ultrasonics, Universidad de Santiago de Chile, January 2009

Semiautomatic contour detection of breast lesions in ultrasonic images with morphological operators and average radial derivative function

W. Gómez^{a*}, L. Leija^a, W. C. A. Pereira^b, A. F. C. Infantosi^b

^aDepartment of Electrical Engineering, CINVESTAV-IPN, Av. IPN 2508, Mexico City, 07000, Mexico

^bBiomedical Engineering Program, COPPE/UF RJ, Av. Horacio Macedo 2030, Rio de Janeiro, 21941-914, Brazil

Abstract

This work presents a computerized lesion segmentation technique on breast ultrasound images. There were applied known techniques such as morphological filtering, Watershed transformation and average radial derivative function. To evaluate the performance of the proposed method, two protocols were established. For the first, the resulting segmentation contours were compared with those of 24 gold standard simulated ultrasound-like images, and, for second, with 36 breast US images manually delineated by two senior radiologists. Further, two evaluation parameters were used: the percentage of coincidence (CP) and the proportional distance (PD). The former indicates the similarity between contours, while the latter express the dissimilarity. The accuracy of the proposed method was evaluated by considering images with CP > 80 % and PD < 10 % as adequately delineated. It was higher than 80% for real images and higher than 88% for simulated images.

Keywords: Average radial derivative; breast ultrasound; morphological operators; segmentation.

1. Introduction

Mammography is currently the best available screening modality for early detection and diagnosis of breast cancer. Periodic screening mammography evaluates asymptomatic women with the goal of discovering early signs of malignant lesions, more specifically microcalcifications. Nevertheless, it is well known that mammography is unable to explore some internal aspects of suspected lesions. Thus, when appropriate, ultrasonographic screening is indicated [1]. Nowadays, breast ultrasound (US) is accepted as the most important adjunct to mammography for patients with palpable masses and normal or inconclusive mammograms. It is particularly useful in distinguishing cystic from non-cystic (solid) breast lesions [2].

Malignant tumors generally infiltrate the surrounding tissue and they present several morphological features associated to malignancy such as: (i) spiculation, a distortion caused by the intrusion of the breast cancer into the

* Corresponding author. Tel.: +52-55-5747-3800; fax: +52-55-5747-3981.

E-mail address: wgomez@cinvestav.mx.

surrounding tissue [3]; (ii) angular margins, obtuse or acute pointed junctions between the mass and surrounding tissue; and (iii) microlobulation, that is frequently associated with angular margins and is characterized by greater than three lobulations of the mass surface [4]. Therefore, analyzing the lesion contour morphology one can provide a diagnostic hypothesis about the tumor malignancy.

However, due to the large overlap in the sonographic appearance of breast lesions, it has been difficult to diagnose them as benign or malignant only by visual inspection of a specialist [5]. To improve diagnosis, a number of researchers have been attempting to develop quantitative methods to build computer-aided diagnosis (CAD) systems.

In a CAD system, the accurate segmentation of breast lesions in ultrasonographies is a difficult task, because of a number of factors like speckle noise and shadows, low or non-uniform contrast of certain structures, and the echogenicity variability of nodules [6]. Thus, to obtain a segmentation method to be used for diagnosis depends on two main aspects: image pre-processing and gray-level threshold selection.

Mathematical Morphology (MM) is a branch of image processing which is useful for analyzing shapes in images. The Morphological Operators (MO) could simplify the image information data, preserving the essential characteristics and removing irrelevant structures. Numerous methods have been developed to segment breast lesions in US images using MO [7]–[9].









In this study, it is proposed a semiautomatic segmentation technique that combines different MO to preprocess the breast US image and the maximization of the average radial derivative (ARD) function to select the optimal gray-level threshold that corresponds to the lesion contour.

2. Material and Methods

2.1. Simulated ultrasound images

To evaluate the segmentation technique performance, simulated ultrasound images were used as a gold standard, containing eight kinds of classical lesion shapes, classified by their cross section. Lesion shapes can be described by the presence, or absence, of “constriction” and “angularity”. The former means convex or indented characteristics, and the latter indicates concave or projecting characteristics (Table 1) [10].

Table 1. Lesion classification according to its shape.

Shape	A	B	Constriction	Angularity
Round/Oval			No	No
Polygonal			No	Yes
Lobulated			Yes	No
Irregular			Yes	Yes

If a typical B-scan US image is examined it could be observed two main patterns. Firstly, on a microscopic scale and within a homogeneous region of tissue, the speckle pattern behaves in a pseudo-random way pixel-to-pixel correlation, which can be viewed as a reflectivity function of identically distributed uncorrelated random variables. On the other hand, on a macroscopic scale, the local average amplitude of the speckle varies piecewise smoothly, remaining uniform or changing slowly in regions of homogeneous tissue but varying sharply at structural or tissue boundaries [11]. Then, a simple way to simulate these different macroscopic and microscopic behaviors of the reflectivity function is to model it as the product of an echogenicity map and a speckle random field with Rayleigh distribution [12], as illustrated in Fig. 1.

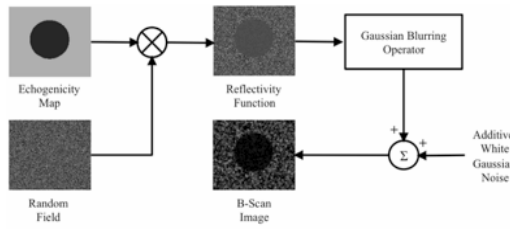


Fig.1 Simulated ultrasound image for a hypothetical anechoic cyst. Multiplying the echogenicity map by a random field with Rayleigh distribution yields a reflectivity function, which, after blurring and adding noise, resembles a typical B-scan image. The gray scales in all of the images represent logarithmically compressed amplitudes.

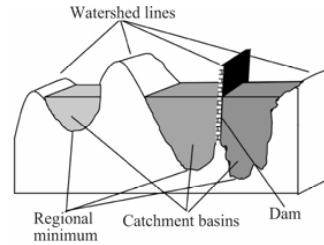


Fig.2 Topographic view of Watershed transformation.

For each lesion shape shown in Table 1, a binary image (used as gold standard) and an ultrasound image were created. The background contrast of the echogenicity map was fixed in -1 dB, and the internal contrast of the simulated lesion was varied -6 dB, -8 dB and -10 dB. The speckle random field has Rayleigh distribution with variance 1. The combination of all controlled characteristics (eight shapes and three contrasts) derived in 24 kinds of ultrasound images. These images were simulated with the purpose of assessing the ability of the segmentation technique to follow the real boundary with controlled levels of irregularity, contrast and speckle noise.

2.2. Breast US image database

In this study, images were acquired with a 7.5–MHz linear array B-mode 40–mm ultrasound probe (Sonoline–Sienna® Siemens) with axial and lateral resolutions of 0.45 mm and 0.49 mm, respectively. Thirty-six US images of breast lesion were acquired at the Cancer National Institute (Rio de Janeiro, Brazil). For each image, two experienced radiologists delineated manually the lesion contours using software designed for that purpose.

2.3. Morphological operators

2.3.1. Morphological Filtering

Three basic requirements are needed when filtering medical images: (i) it should preserve lesion boundaries and structure details; (ii) it should suppress noise in homogenous regions; and (iii) it should enhance edge information [13].

As previously mentioned, US images are characterized by speckle artifact, which degrades the image by concealing fine structures and reducing the signal to noise ratio (SNR) [14]. Moreover, in many cases, it is harder to locate the edges of different elements due to the low contrast between the structures to be segmented and the background. Therefore, it is necessary to remove speckle and enhance the edges between distinct regions before the segmentation procedure.

The basic morphological filters are the morphological opening γ_B and the morphological closing φ_B with a given structuring element (SE) B , and they are defined as:

$$\gamma_B(f) = \delta_B[\varepsilon_B(f)] \tag{1}$$

$$\varphi_B(f) = \varepsilon_B[\delta_B(f)] \tag{2}$$

where \hat{B} is the transposed SE, and ε_B and δ_B are the operations of erosion and dilation, respectively [15].

Another class of filters is composed by the opening and closing by reconstruction. When filters by reconstruction are built, the basic geodesic transformation, the geodesic dilation and the geodesic erosion, are iterated until idempotence is reached. Where the geodesic dilation and geodesic erosion are given by $\delta_f(g) = f \wedge \delta(g)$ with $g \leq f$ and $\varepsilon_f(g) = f \vee \varepsilon(g)$ with $g \geq f$, respectively. When the function g is equal to the erosion or the dilation of the original function, it is obtained the opening and closing by reconstruction:

$$\tilde{\gamma}_B(f) = \lim_{n \rightarrow \infty} \delta_f^n[\varepsilon_B(f)] \quad (3)$$

$$\tilde{\varphi}_B(f) = \lim_{n \rightarrow \infty} \varepsilon_f^n[\delta_B(f)] \quad (4)$$

Therefore, the opening by reconstruction $\tilde{\gamma}$ of an image f with $SE = B$, is defined as the erosion of f with the $SE = B$ followed by the geodesic dilation iterated until stability is reached, where \wedge is the point-wise minimum. The effect of $\tilde{\gamma}$ is to remove all structures in an image that are both smaller than the SE and brighter than the surroundings.

On the other hand, the closing by reconstruction $\tilde{\varphi}$ of an image f , with $SE = B$, is defined as the dilation of f with $SE = B$, followed by the geodesic erosion iterated until idempotence is reached, where \vee is the point-wise maximum. The result of $\tilde{\varphi}$ is to remove all structures that are both smaller than the SE and darker than the surroundings.

2.3.2. Watershed transform

The Watershed transform is the method of choice for image segmentation in the field of MM, and can be considered as a region-based segmentation approach.

The intuitive idea underlying this method comes from Geography. Imagine that a landscape or topographic relief is being immersed in a lake, with holes pierced in local minima. Basins (also called “catchment basins”) will be filled up with water starting at these local minima, and, at points where water coming from different basins meets, dams are built. When the water level has reached the highest peak in the landscape, the process is stopped. As a result, the landscape is partitioned into regions or basins separated by dams, called watershed lines or simply watersheds (see Fig. 2) [16]. In agreement with this concept, the Watershed transform could be used to separate modal regions in an image histogram.

2.3.3. Minima imposition

The minima imposition is a kind of morphological filtering that requires a set of markers that are related to dark objects. In the case of the semiautomatic segmentation algorithm, the user defines manually this marker at the lesion center.

To perform the minima imposition, firstly, it is computed the point-wise minimum between the input image, f , and the marker image, $f_m: f \wedge f_m$. By doing so, minima are created at locations corresponding to the markers, assuring that the resulting image is lower or equal to marker image. The last step consists in a morphological reconstruction by erosion of $f \wedge f_m$ from the marker image f_m [15].

2.4. Breast US image preprocessing by MO

In order to remove speckle in the US image while preserving important information from lesion boundaries, an Alternating Sequential Filter (ASF) is applied to the breast US image. The ASF performs a closing by reconstruction followed by an opening by reconstruction using a disk (5-pixel radius) SE [see Fig. 3(a)]:

$$ASF_B(f) = \tilde{\gamma}[\tilde{\varphi}_r(f)] \quad (5)$$

Then, it is performed a morphological opening after closing (vertical line SE with 3-pixels) on the histogram of the filtered image with the purpose of removing irrelevant peaks [see Fig. 3(b)]. In addition, the filtered histogram is inverted to find the regional minimum [see Fig. 3(c)], and the Watershed transform is used to define modal regions of the inverted filtered histogram [see Fig. 3(d)].

Each region is numerically labeled and sorted in crescent order to reconstruct a new image characterized by a small number of gray levels [see Fig. 3(e)]. Then, to enhance the lesion from its background, a minima imposition operator is applied [see Fig. 3(f)].

To assure that pixels inside the lesion have smaller values than the background, all of them should be marked as belonging to the lesion. Note that this marked point is the only information defined manually for the semiautomatic segmentation algorithm.

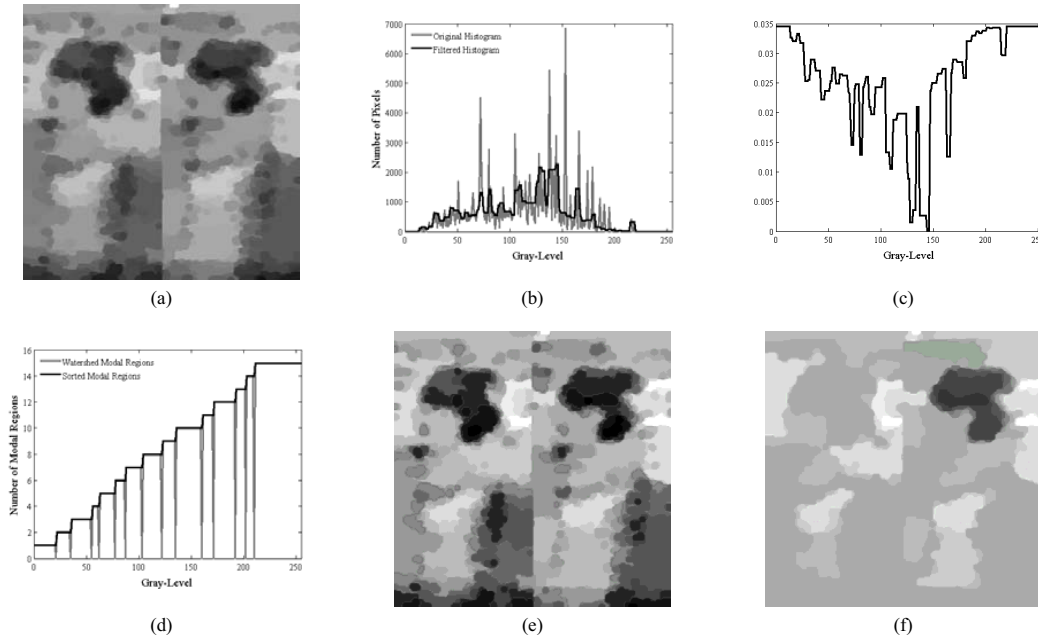


Fig.3 Morphological pre-processing procedure of the breast US image. (a) Alternating Sequential Filtering - ASF, (b) histogram of the filtered image (gray line) and filtered histogram (black line), (c) inverted filtered histogram, (d) modal regions defined by Watershed transform (gray line) and sorted modal regions (black line), (e) reconstructed image with small number of gray levels, and (f) minima imposition, the marker is a point manually defined inside the lesion.

2.5. Lesion segmentation

The main idea is to obtain potential lesion margins that will be used in the evaluation of a gradient-base utility function to find the definitive lesion contour.

By observing the gray-levels related to the lesion, it is possible to make an analogy with the jigsaw puzzle, where the gray-levels represent different shapes or pieces that have to be fitted together to assemble the lesion. If these pieces are iteratively combined, new shapes will be formed and each one represents an approximation of the definitive shape. To do this, a thresholding process is performed on the imposed image to create binary subsets that represent potential lesion margins (region growing scheme) [Fig. 4(a)].

The utility function used in the segmentation algorithm is the Average Radial Derivative (ARD), which gives the average directional derivative in the radial direction along the contour, and it is defined as [17]:

$$ARD(\Gamma) = \frac{1}{N} \sum_{p \in \Gamma} \nabla \tilde{I}(\hat{p}) \cdot r(\hat{p}) \quad (6)$$

where Γ is the discretized potential lesion margin, N is the number of points in Γ , $\nabla \tilde{I}$ is the gradient of the preprocessed image by MO, $\hat{r}(\hat{p})$ is the unit vector in the radial direction from the point defined manually inside the lesion to the point $\hat{p} = (x, y)$, and \cdot is the dot product between vectors. The potential margin that maximizes the ARD function defines the definitive lesion contour [see Fig. 4(b) and 4(c)].

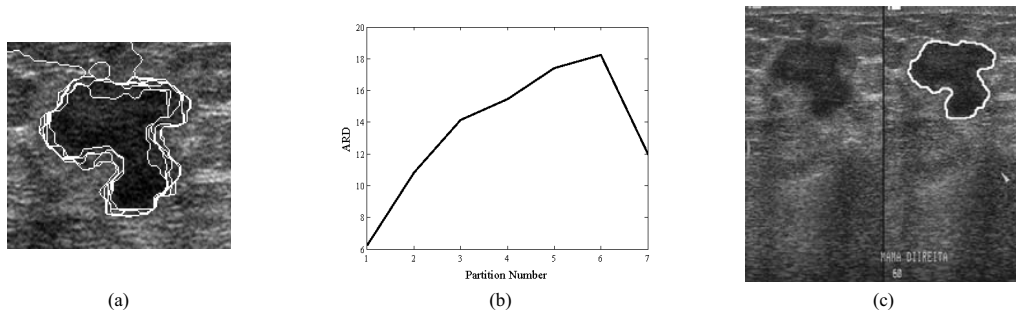


Fig.4 (a) Potential lesion margins (white lines) derived from the region growing scheme. (b) ARD curve maximized at the partition number 6 and (c) the respective detected lesion contour (white line).

2.6. Performance evaluation

In order to evaluate the accuracy of the segmentation method (SM), a set of 36 breast US images was used. All the lesions had their contour manually delineated by two specialists. Moreover, the SM was also applied to a set of 24 simulated ultrasound-like images (with known contours). Both human manually delineated and simulated contours were used as gold standards for the sake of comparison.

Two parameters were used to evaluate the SM performance. The first one is the coincidence percentage (CP), which measures the similarity between the proposed segmentation technique and the gold standard, that is:

$$CP(S_1, S_2) = \frac{\text{Area}(S_1 \cap S_2)}{\text{Area}(S_1 \cup S_2)} * 100 \quad (7)$$

where S_1 and S_2 are the two segmentations to be compared, and the symbols \cap and \cup indicate the areas intersection and union (in pixels), respectively. When S_1 and S_2 have the same geometrical characteristics and position CP is equal to 100 % [6].

The second parameter is the proportional distance (PD), which expresses not only if two contours differ in the number of pixels but rather how far their pixels are. Hence, PD can be seen as a measure of dissimilarity. Let S_1 and S_2 be the two segmentations to be compared, and C_1 and C_2 their respective contours, the proportional distance between them is given by [6]:

$$PD(S_1, S_2) = \frac{\frac{\sum_{x_i \in C_1} d(x_i, C_2)}{|C_1|} + \frac{\sum_{x_i \in C_2} d(x_i, C_1)}{|C_2|}}{2\sqrt{\frac{\text{Area}(RS)}{\pi}}} * 100 \quad (8)$$

where the numerator calculates the mean distance from all the pixels of C_1 to the contour C_2 , and vice-versa. $d(x_i, C)$ is the geometrical distance (in points) from a point x_i to the contour C , which has a number of points denoted as $|C|$. The denominator is a normalized factor which turns this parameter independent on scale changes, being RS the segmentation reference. With such a definition, if C_1 and C_2 are congruent, $PD = 0$ %.

For a simulated image, PD (or CP) was taken as an average of 30 values calculated from simulations carried out with the same characteristics (e.g. irregular shape and -10 dB internal contrast), but with random speckle distribution.

3. Results

Examples of the proposed segmentation method applied to simulated and real images are depicted in Fig. 5 in which the corresponding reference segmentations (contours) are also shown. As one can note in these examples, the contours are almost the same for the simulated images and there is a slightly difference for real images.

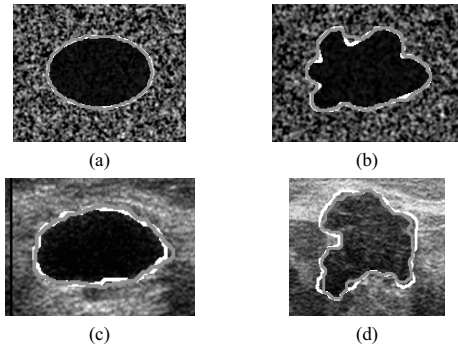


Fig.5 Comparison of the computerized segmentations (gray line) and the reference delineations (white line) obtained from simulated ultrasound images (a) CP = 97.18 %, PD = 1.28 %, and (b) CP = 96.05 %, PD = 1.59 %; and manually delineated contours by the specialists (c) CP = 92.53 %, PD = 3.35 % and (d) CP = 87.50 %, PD = 4.74 %.

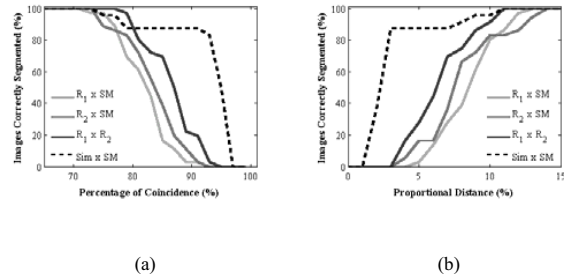


Fig.6 Performance curves for the parameters (a) CP and (b) PD applied to the segmentation method for 36 breast US images and 24 simulated images. It can be seen the percentage of the simulated and real images at different CP and PD values with SM and the radiologists manually contours.

Also from the curves of Fig. 6, it is possible to establish a threshold from which the segmentation technique could be considered as adequate. Table 2 summarizes the results of considering the proposed segmentation method as successful if both CP is higher than 80 % and PD lower than 10 %.

Table 2. Percentage of images that follow the established thresholds for CP > 80 % and PD < 10 %.

Test*	Percentage of images	
	CP	PD
R ₁ × SM	67	81
R ₂ × SM	81	83
R ₁ × R ₂	92	92
Sim × SM	88	96

*SM = Segmentation Method, R1 = Radiologist-1, R2 = Radiologist-2 and Sim = Simulated.

These findings indicate that there exist little variations between the contours delineated by the radiologists. This statement is also valid when comparing those contours with the computerized segmentation here proposed. Moreover, for the ultrasound-like images, it is observed a high agreement between the SM contours and the simulated patterns.

4. Discussion and Conclusion

It was presented a semiautomatic segmentation method for breast US lesions. It was used known techniques such as morphological filtering, Watershed transform, minima imposition or average radial derivative function. The combination of these techniques provides quite satisfactory results in the segmentation of very complex data such as US images (as can be seen from the percentages of Table 2).

In this work, the simulated images were created with ultrasonic characteristics to evaluate the accuracy of the computerized segmentation technique to follow the real boundary of the lesion. The noise added to the images is multiplicative Rayleigh distributed, which is similar to the speckle pattern presented in US images. Also, the

simulated lesions have typical shapes classified by their cross section as regular, polygonal, lobulated or irregular. This kind of US images approach has been previously proposed by Alvarenga *et al.* [7] to assess the segmentation algorithms. In these works the authors developed simulated images based in gears with 8 and 16 teeth, varying both contrast ratio and noise power between the gear and its background. However, these images did not adequately simulate the typical US characteristics. First, the noise added to the images is uniform speckle, which is not well fitted for this application; second, the shapes simulated are not classical lesion shapes; and third, the images are not logarithmically compressed. In this sense, our simulated images presented an improvement because there were simulated variables that depict real ultrasonographies.

Mathematical Morphology provides powerful tools to analyze the shape and sizes of the objects, and its concepts can be applied in medical images. In this work the segmentation technique steps are: (i) morphological filtering, (ii) reducing the number of gray-levels of the image applying MO to the image histogram, (iii) minima imposition to enhance the lesion, (iv) region growing scheme and (v) selection of the gray-level threshold for lesion segmentation by the maximization of the ARD function.

The SM time-processing was assessed using the 36 breast US data set. The segmentation time depends directly on image size and also on the shape and size of the lesion. All images in database have 378×374 pixels. The average time processing was 6.42±2.24 seconds. Therefore, the segmentation technique based in MO is fast enough to be implemented in real-time, and it is capable of delineating lesion with a good level of accuracy, according to the performance evaluation parameters we used. Encouraged by these results, our current efforts are to include this technique as part of the development of a CAD system to detect and diagnose breast lesion on US images.

5. Acknowledgements

To Consejo Nacional de Ciencia y Tecnología (CONACYT, Mexico) and the Ministries of Science and Technology and Health (MCT-CNPq/MS-SCTIE-DECIT/CT no. 06/2005, project no. 401274/2005-5), for the financial support.

References

- [1] D. J. Winchester, "Atlas of Clinical Oncology: Breast Cancer, American Cancer Society," BC Decker Inc. (2000) 41–63.
- [2] H. M. Zonderland, E. G. Coerkamp, M. J. Vijver, and A. E. Voortuisen, "Diagnosis of Breast Cancer: Contribution of US as an Adjunct to Mammography," *Radiology* 213 (1999) 413–422.
- [3] S. F. Huang, R. F. Chang, D. R. Chen, and W. K. Moon, "Characterization of Spiculation on Ultrasound Lesions," *IEEE Trans. Med. Imaging* 23 (2004) 111–121.
- [4] R. F. Chang, W. J. Wu, W. K. Moon, and D. R. Chen, "Automatic Ultrasound Segmentation and Morphology Based Diagnosis of Solid Breast Tumors," *Breast Cancer Res. Tr.* 89 (2005) 179–185.
- [5] M. L. Giger, "Computer-Aided Diagnosis of Breast Lesions in Medical Images," *Comput. Sci. Eng.* 2 (1999) 39–45.
- [6] M. Alemán-Flores, L. Álvarez, and V. Caselles, "Textured-Oriented Anisotropic Filtering and Geodesic Active Contours in Breast Tumor Ultrasound Segmentation," *J. Math. Imaging Vis.* 28 (2007) 81–97.
- [7] A. V. Alvarenga, A. F. C. Infantosi, C. M. Azevedo, and W. C. A. Pereira, "Application of Morphological Operators on the Segmentation and Contour Detection of Ultrasound Breast Images," *Braz. J. Biomed. Eng.* 19 (2003) 91–101.
- [8] A. F. C. Infantosi, L. M. S. Luz, W. C. A. Pereira, and A. V. Alvarenga, "Breast Ultrasound Segmentation Using Morphological Operators and a Gaussian Function Constraint," in *Proc. 14th NBC* (2008) 520–523.
- [9] Y. L. Huang and D. R. Chen, "Watershed Segmentation for Breast Tumor in 2-D Sonography," *Ultrasound Med. Biol.* 3 (2004) 625–632.
- [10] E. Ueno, T. Shiina, and M. Kubota, "Research and Development in Breast Ultrasound," Springer (2005) 55–56.
- [11] J. Ng, R. Prager, N. Kingsbury, G. Treece, and A. Gee, "Wavelet Restoration of Medical Pulso-Echo Ultrasound Images in a EM Framework," *IEEE Trans. Ultrason. Ferroelectr. Freq. Control* 54 (2007) 550–568.
- [12] B. Cohen and I. Dinstein, "New Maximum Likelihood Motion Estimation Schemes for Noise Ultrasound Images," *Pattern Recognition* 32 (2002) 455–463.
- [13] G. Gerig, O. Kubler, R. Kikinis, and F. A. Jolesz, "Nonlinear Anisotropic Filtering of MRI Data," *IEEE Trans. Med. Imaging* 11 (1992) 221–232.
- [14] Y. Yu and S. T. Acton, "Speckle Reduction Anisotropic Diffusion," *IEEE Trans. Med. Imaging* 11 (2002) 1260–1270.
- [15] P. Soille, "Morphological Image Analysis," 2nd ed., Heidelberg: Springer-Verlag (2002).
- [16] J. Roerdink and A. Meijster, "The Watershed Transform: Definitions, Algorithms and Parallelizations Strategies," *Fundamenta Informaticae* 41 (2001) 187–228.
- [17] K. Horsch, M. L. Giger, L. A. Venta and C. J. Vyborny, "Automatic segmentation of breast lesions on ultrasound," *Med. Phys.* 28 (2001) 1652–1659.